Diffractive scattering

E.A. De Wolf§

CERN, European Laboratory for Particle Physics, 1211 Geneva 23, CH

E-mail: eddi.dewolf@ua.ac.be

Abstract. We discuss basic concepts and properties of diffractive phenomena in soft hadron collisions and in deep-inelastic scattering at low Bjorken-x.

1. Introduction

Diffractive scattering, or Pomeron physics, has made a spectacular come-back with the observation of Large Rapidity Gap events at the HERA ep collider and similar studies at the highest energy hadron colliders. It has become a field of intense research and many detailed aspects were reviewed at this Workshop, as well as elsewhere [1, 2].

To develop a general phenomenology of very high energy scattering and diffraction, which originated from studies of predominantly soft hadron hadron collisions, it is tempting and traditional to start from a t-channel formalism based on Regge theory. For deep-inelastic scattering (DIS) and hard diffractive processes this leads to the simple (and popular) Pomeron picture as first proposed by Ingelman and Schlein [3]. Although Regge theory is perfectly valid and beautiful, based on very general properties of the scattering amplitudes, it is plagued by many problems in practical applications which, as happened in the past, severely limit its predictive power. Apart from the fundamental theoretical question how to derive the theory as a strong-coupling limit of QCD, it provides little insight into the relation between properties of the final states, the structure of the theory and the physical meaning of its parameters. This becomes particularly severe when the formalism is used outside its traditional domain of application, such as in deep-inelastic scattering.

In this paper, we shall mainly adopt an s-channel picture of diffraction. Diffractive scattering is explained by the differential absorption by the target of the large number of states which coherently build up the initial-state hadron or (virtual) photon and scatter with different cross sections. Such an approach incorporates from the outset basic quantum mechanics and unitarity and permits, at least conceptually, a unified treatment of hadron and virtual photon scattering. It will allow us to appreciate the close inter-relation between the dynamics of high-energy hadronic and deep-inelastic

§ Also at University of Antwerpen, Physics Department, Universiteitsplein 1, B-2610 Antwerpen, Belgium

diffraction (DDIS) at very small Bjorken-x and to understand that long-distance physics plays a very important role in both. It is also the approach used in the most successful of the present theoretical models [2].

The main thrust of the paper will be to argue that the physics can be understood on the basis of a surprisingly small number of dynamical ingredients. This in turn leads to a view of the collision dynamics which is simple enough to help develop intuition, provide physical insight and suggest fruitful avenues of research. The latter aspect, although briefly touched upon, could not be fully developed here, for lack of space-time, but will be discussed elsewhere. The paper is mainly addressed to experimentalists entering the field and we hope it will broaden their view of the subject. No originality is claimed in the presentation of the material although any errors of interpretation should be attributed solely to the author.

2. Preliminaries

The standard kinematical variables to describe ep DIS are depicted in figure 1a. The centre-of-mass energy squared of the ep system is $s = (P+k)^2$, with P and k the initial-state four-momenta of the proton and electron (or positron), respectively. W, the CMS energy of the virtual-photon proton system, is given by $W^2 = (P+q)^2$. The photon virtuality Q^2, the Bjorken variables x and y are defined as

$$q^2 = -Q^2 = (k-k')^2, \quad x = \frac{Q^2}{2\ P\cdot q} = \frac{Q^2}{W^2+Q^2-m_p^2}, \quad y = \frac{P\cdot q}{P\cdot k}. \quad (1)$$

For the semi-inclusive or "rapidity-gap" process presented in figure 1b, where a baryon with four-momentum P' is detected in the final state, one defines the additional variables

$$t = (P-P')^2; \quad \xi = \frac{Q^2+M_X^2-t}{Q^2+W^2}; \quad \beta = \frac{Q^2}{Q^2+M_X^2-t} = \frac{x}{\xi}, \quad (2)$$

In present experiments, $|t|$ is small and can be neglected in (2). The variable ξ is approximately equal to the fractional energy-loss suffered by the incident proton. In full analogy with the relation between $F_2(x,Q^2)$ and the total $\gamma^\star p$ cross section, the differential cross section for a semi-inclusive DIS process (figure 1b), integrated over t, can be written as

$$\frac{\mathrm{d}^3\sigma}{\mathrm{d}x dQ^2 \mathrm{d}\xi} = \frac{4\pi\alpha_{em}^2}{x\ Q^4}\left[1-y+\frac{y^2}{2(1+R)}\right]\ F_2^{SI(3)}(\xi,x,Q^2). \quad (3)$$

which defines the semi-inclusive structure function $F_2^{SI(3)}(\xi,x,Q^2)$; α_{em} is the QED coupling. Alternatively, in measurements of the diffractive contribution to $F_2(x,Q^2)$, one often uses the definition

$$\frac{d^3\sigma}{d\beta dQ^2 d\xi} = \frac{4\pi\alpha_{em}^2}{\beta\ Q^4}\left[1-y+\frac{y^2}{2(1+R)}\right]\ F_2^{D(3)}(\xi,\beta,Q^2). \quad (4)$$

replacing x by β in (3). $R = \sigma_L/\sigma_T$ is the ratio of the cross sections for longitudinally and transversely polarized virtual photons. For small enough y, R can be neglected.

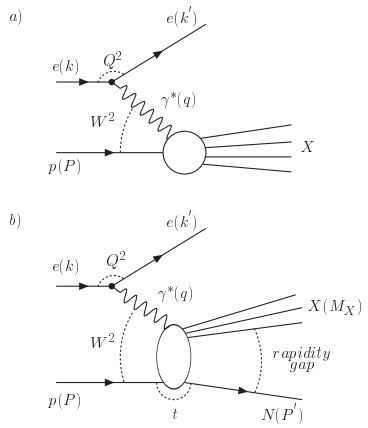

Figure 1. Kinematic variables (a) for the reaction $e\ p \to e\ X$; (b) for the semi-inclusive reaction $e\ p \to e\ N\ X$ with a rapidity gap.

Equations (3) and (4) are equivalent since they represent the same experimental data. From an experimental point of view, there is no a priori reason to prefer one over the other and both should be measured.

2.1. Regge formalism

Since the Regge formalism is so often used in present analyses of diffractive HERA data, it is useful to briefly recall its main ingredients and predictions.

For scattering of two hadrons a and b at a squared center-of-mass energy $s \gg m_{a,b}^2,\ t$, Regge phenomenology predicts that

$$\sigma_{\mathrm{T}}(ab \to X) \quad \sim s^{\alpha_{I\!P}(0)-1} = s^{\epsilon}, \tag{5}$$

$$\frac{\mathrm{d}^2\sigma_{\mathrm{el}}}{\mathrm{d}t}(ab \to ab) \quad = \frac{\sigma_{tot}^2(ab)}{16\pi} e^{2(b_0^{el}+\alpha'_{I\!P}\ln s)t}, \tag{6}$$

$$\frac{\mathrm{d}^2\sigma^{\mathrm{DD}}}{\mathrm{d}t\mathrm{d}M_X^2}(ab \to Xb) \sim \frac{1}{M_X^2}\left(\frac{s}{M_X^2}\right)^{2(\alpha_{I\!P}(0)-1)} e^{2(b_0^D+\alpha'_{I\!P}\ln\frac{s}{M_X^2})t}; \tag{7}$$

where $\alpha_{I\!P}(t) = \alpha_{I\!P}(0)+\alpha'_{I\!P}\,t = 1+\epsilon+\alpha'_{I\!P}\,t$ is a parameterization of the Pomeron trajectory. In Regge theory $\alpha_{I\!P}(t)$, i.e. $\alpha_{I\!P}(0)$ and $\alpha'_{I\!P}$ must be "universal" i.e. independent of the species of the incident particles.

From (6) follows that $B(s) = \mathrm{d}(\ln \mathrm{d}\sigma/\mathrm{d}t)/\mathrm{d}t|_{t=0}$, the slope of the t distribution, increases with $\ln s$ with a rate determined by $\alpha'_{I\!P}$. This is known as shrinkage. The term b_0^{el} originates from the Regge residue factors (in an exponential approximation) and is independent of s. In impact parameter ($\vec{b}$) space, the $ab \to ab$ Regge amplitude corresponds to scattering off a Gaussian interaction region with transverse extension $\langle\vec{b}^2\rangle = 2B(s)$.

The collision can visualized in the impact-parameter plane. The scattering profile is a disc with a b-dependent opacity, the mean radius of the disc being proportional to $\sqrt{B(s)}$, and increases with s with a rate of growth determined by $\alpha'_{I\!P}$, estimated to be

≈ 0.25 GeV^{-2} [4]. At the same time, the opacity at fixed b is likely to increase too. In a perturbative QCD picture, this corresponds to an increase of the gluon density in the target or, in the proton rest frame, with an increase of the interaction probability.

Equation (7), which assumes triple-Pomeron dominance, predicts a power-law universal dependence of the single-diffractive cross section on ξ, the fractional proton energy-loss, given by

$$\left.\frac{\mathrm{d}^2\sigma}{\mathrm{d}t\ d\xi}\right|_{t=0} \sim \frac{1}{\xi^{(1+\delta)}} \qquad \text{with} \quad \delta \ll 1. \tag{8}$$

From (5)-(7) also follows that both $\sigma_{\rm el}/\sigma_{\rm T}$ and $\sigma^{\rm DD}/\sigma_{\rm T}$ increase as s^{ϵ}. This eventually leads to violation of unitarity since ϵ is positive. The total diffractive cross section, $\sigma_{\rm T}^{\rm DD}$, grows a $s^{2\epsilon}$.

3. Experimental results on total and elastic cross sections

3.1. Energy dependence of hadronic total cross sections

Total hadron-hadron cross sections, $\sigma_{\rm T}$, have been measured for many combinations of hadrons. Above $\sim$ 20 GeV all hadronic cross sections rise with s. In [5] it was observed that hadron-hadron (and γp) cross sections grow in an similar way at high s. An economical parameterization is a sum of two power-law terms in s

$$\sigma_{\rm T} = X s^{\epsilon} + Y\, s^{\epsilon'}, \tag{9}$$

where the constants X and Y depend on the reaction, but not ϵ and ϵ'. In the Regge framework, the two terms in (9) correspond to Pomeron and "ordinary" Regge exchanges, associated with known resonances. The value of ϵ is not very precisely established. Various recent "global" fits find the data to be compatible with ϵ in the range $0.08 - 0.1$ [5, 6, 7]; ϵ' is found to be ~ -0.5 [5]. One should also note that the present data cannot discriminate between "simple-pole" fits, such as (9) and equally valid fits to $\log^2 s$ and $\log s$ (or $e^{2\sqrt{\log s}}$) functional dependences.

Although the significance of (9) has been over-emphasized, the "universal" high-energy behaviour of the total hadronic cross sections is an important observation which calls for deeper understanding. It also raises the question (not addressed in Regge theory) which particular final states are responsible for this increase.

3.2. The $\gamma^\star p$ total cross section at HERA

The measurement of the total $\gamma^\star p$ cross section as a function of Q^2 and W is one of the major achievements of the experiments at HERA. Parameterizing its W-dependence, at fixed Q^2, as $\sigma_{tot}^{\gamma^\star p} \sim (W^2)^{\lambda_{tot}}$, one finds (figure 2) that λ_{tot} increases linearly with $\log(Q^2)$ from a value $\simeq 0.08$ at low Q^2, the same as in hadron-hadron interactions, to $\simeq 0.35$ at the highest Q^2. Remembering that $1/\sqrt{Q^2} = R_\gamma^\star$ determines the transverse distance which the photon can resolve, we note that for small Q^2 (large $R_\gamma^\star$) the cross section has a hadron-like increase with W: the photon acts like a hadron. With increasing

Q^2, the rise with W becomes stronger: the photon "shrinks" and becomes more and more point-like. If interpreted in terms of Regge exchanges, it is clear that for virtual photon proton scattering "universality" of the trajectory parameter $\alpha_{I\!P}(0)$ no longer holds: $\alpha_{I\!P}(0)$ depends on Q^2. A continuous transition occurs from the "soft" regime to that where a "small-size" $\gamma^\star$ hits a proton.

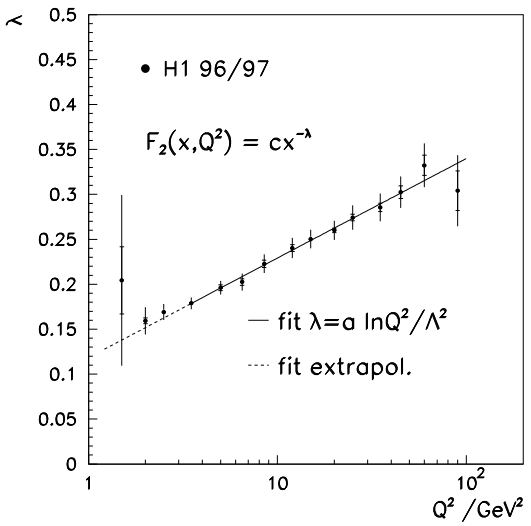

Figure 2. The exponent λ_{tot} in $\sigma_{tot}^{\gamma^\star p} \sim (W^2)^{\lambda_{tot}}$, versus Q^2. The full line shows a fit to the form indicated with $a = 0.0481 \pm 0.0013(\text{stat}) \pm 0.0037(\text{syst})$ and $\Lambda = 292 \pm 20(\text{stat}) \pm 51(\text{syst})$ MeV. Extrapolation to $Q^2 = 0.48$ GeV^2 gives a value of 0.08 (H1)[54].

3.3. Elastic scattering and forward slope

3.3.1. Hadron hadron interactions. Figure 3a shows data on the forward elastic slope in pp and $\overline{p}p$ interactions. The shrinkage of the diffractive peak as $\sqrt{s}$ increases is experimentally well-established and agrees with Regge expectations. The measured values of $B(s)$ correspond to what is expected for (optical) diffraction on a "black" fully absorbing disk of radius R for which $B = R^2/4$. However, for scattering on a black (fully absorbing) disk, $\sigma_{\rm el}/\sigma_{\rm T} = 1/2$, whereas experiment (figure 3b), shows much smaller values even at the highest energies. One can conclude that the proton is semi-transparant, even at zero impact parameter [8]. This can be understood since the wavefunctions of the incident hadrons are a superposition of states, some of which are strongly absorbed, while others pass through almost unaffected. Such a mixture of states with very different absorption probabilities will be essential for inelastic diffraction to occur, see section 5.2.

3.3.2. Real and virtual photon quasi-elastic scattering. Among the many results now available (for a review see [1, 9, 10]), figure 4 shows, as an example, recent ZEUS measurements of the W-dependence of elastic ρ^0 electroproduction as a function of

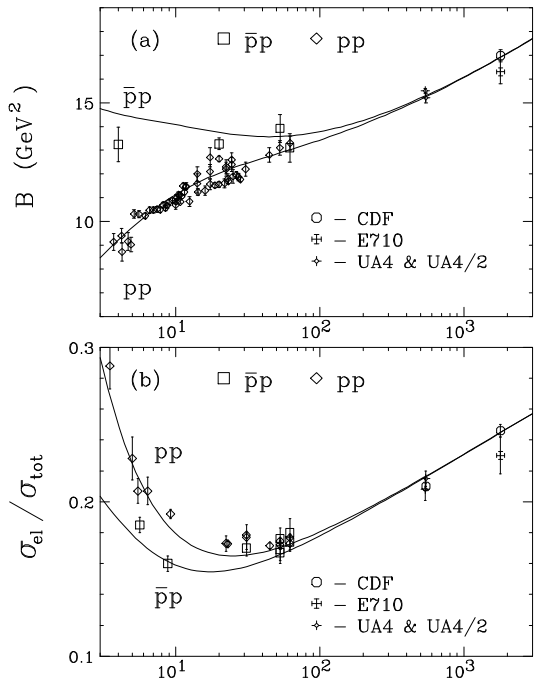

Figure 3. (a) slope parameter $B(s)$, (b) ratio of elastic to total cross section versus $\sqrt{s}$ for $\bar{p}p/pp$ interactions. The dashed lines are standard Regge fits, the solid lines are fits after eikonalization of the elastic scattering amplitude. For details see [7]).

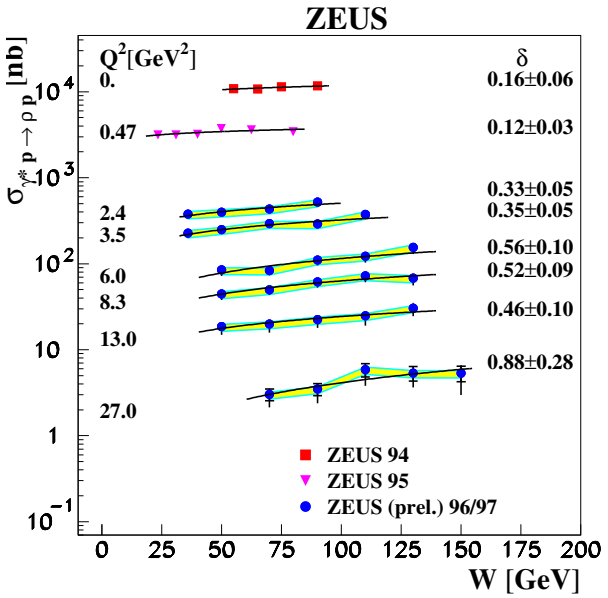

Figure 4. W dependence of the cross section $\sigma(\gamma^* p \to \rho^0 p)$ for various Q^2 values. The data for $Q^2 < 1$ GeV^2 obtained previously [55] are also shown. The dashed lines show a fit with $\sigma_{\gamma^* p \to \rho^0 p} \sim W^\delta$. The shaded area indicates normalization uncertainties due to proton dissociation background. From [11].

Q^2 [11]. For each Q^2 interval, the cross section is assumed to be of the form W^δ. In the same manner as for the $\gamma^\star p$ total cross section, the data suggest a marked increase of δ when Q^2 enters a regime where pQCD becomes relevant. However, the errors remain sizable and, in W-regions where the DIS data overlap ($3.5 \leq Q^2 \leq 13.0$ GeV^2), the Q^2-dependence of δ is statistically not yet very significant. Measurements at larger Q^2 are needed to clarify this important issue.

As to the shape of the diffractive peak, figure 5 shows a compilation [12] of the slope B, at fixed W, as a function of an effective scale, $Q^2_{eff} = Q^2 + m^2_{\rm V}$, for various vector mesons with mass $m_{\rm V}$. The slope becomes smaller with increasing Q^2_{eff}. In the photoproduction region, $Q^2_{eff} = 0$, the slopes for ρ and ω are quite similar to those observed in proton-proton scattering, see figure 3. At higher Q^2_{eff}, they are considerably smaller, approximately half of that observed in proton-proton scattering. The effective interaction region reduces to about that of a single proton, as expected for a projectile which becomes more point-like as Q^2 grows. At the same time the total cross section itself grows faster than in hadron interactions. If the transverse size of the interaction region is not increasing, the latter observation implies that the absorption of the incoming projectile's wavefunction by the target, which causes elastic diffraction, is increasing. Since the probability of absorption cannot exceed unity, saturation (i.e. a levelling off of the W increase) of the total cross section is bound to occur at some high W.

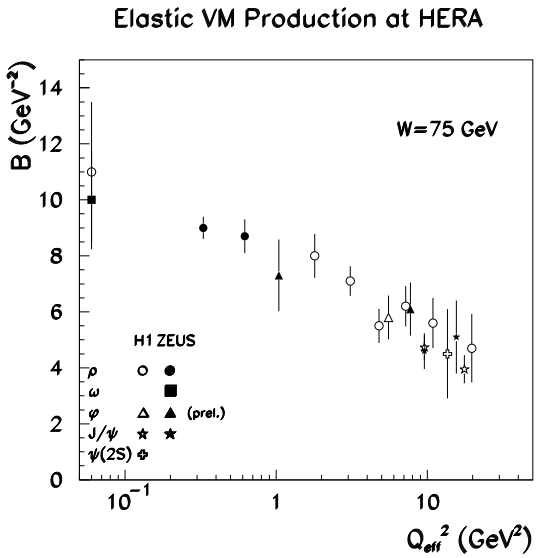

Figure 5. Slope parameter $B(s)$ as a function of Q^2_{eff}; $Q^2_{eff} = Q^2$ for ρ and ω, $Q^2_{eff} = Q^2 + M^2_\phi$ for ϕ, $Q^2_{eff} = Q^2 + M^2_{J/\Psi}$ for J/Ψ. From [12]

For elastic J/ψ photoproduction, ZEUS recently measured the differential cross-section, $d\sigma/dt \propto (W^2)^{2\alpha_{I\!P}(t)-2}$, in the energy-range $20 < W < 290$ GeV, and $|t| < 1.25$ GeV^2. From the t-slope in bins of W yielding e.g. $B = 4.3 \pm$

$0.08\,(\mathrm{stat})^{+0.16}_{-0.41}\,(\mathrm{syst})$ GeV^{-2} at $W = 90$ GeV, one derives (see [13]) $\alpha_{I\!P}(0) = 1.201 \pm 0.013\,(\mathrm{stat})^{+0.003}_{-0.011}\,(\mathrm{syst})$ and $\alpha'_{I\!P} = 0.126 \pm 0.029\,(\mathrm{stat})^{+0.015}_{-0.028}\,(\mathrm{syst})$ GeV^{-2}. The latter value implies small but not negligible shrinkage. This was predicted in [14].

A recent first-time ZEUS measurement [11] of the leading trajectory parameters from exclusive ρ production in DIS, $\gamma^\star p \to \rho^0 p$, ($1 < Q^2 < 40$ GeV^2), yielded $\alpha_{I\!P}(0) = 1.14 \pm 0.01\,(\mathrm{stat})^{+0.03}_{-0.03}\,(\mathrm{syst})$, $\alpha'_{I\!P} = 0.04 \pm 0.07\,(\mathrm{stat})^{+0.13}_{-0.04}\,(\mathrm{syst})$ GeV^{-2}. While not conclusive, given the errors, the measurement suggests a smaller value of $\alpha'_{I\!P}$ than that of the "soft" Pomeron ($\alpha'_{I\!P} \approx 0.25$ GeV^{-2}).

From a measurement of the spin-density matrix of the ρ^0 decay, ZEUS [11] also extracted σ_L/σ_T, the ratio of the cross section for longitudinally and transversely polarized $\gamma^\star$, as a function of Q^2 and W. The ratio strongly increases with Q^2 but is found to be independent of W, a somewhat surprising result given the expectation that at large Q^2 the average transverse size of the longitudinally polarized $\gamma^\star$ is much smaller than that of a transversely polarized $\gamma^\star$ [15].

In summary, although more precise measurements are evidently needed, and forthcoming, the present data on total and elastic differential cross sections suggest a clear trend. As for real hadrons, for near-on-shell photons fluctuating into light vector mesons, (ρ, ϕ) and which have large (order 1 fm) transverse extensions, inversely proportional to the Compton wavelength of the light quarks in the meson, the effective Pomeron trajectory $\alpha_{I\!P}(t)$ is close to that of soft collisions. For heavier vector mesons (e.g. J/ψ) which are characterized by a smaller transverse size, or in DIS, present data provide some indication for a weaker shrinkage, with $\alpha'_{I\!P}$ smaller than the "soft" value 0.25 GeV^{-2}. At the same time, the effective intercept $\alpha_{I\!P}(0)$ grows with decreasing size $R^\star_\gamma$. The transition from the soft hadron-like regime to DIS is a smooth one.

4. Inelastic diffraction

4.1. Experimental signatures

In contrast to forward elastic scattering, which beautifully reflects the wave-nature of the particles, the phenomenon of diffraction dissociation, *predicted* by Good and Walker [16], has no classical analogue. It corresponds to quasi-elastic scattering where one (single diffraction) or both (double diffraction) of the incident hadrons is excited into a higher mass state retaining its quantum numbers. In single diffraction, the need to maintain the coherence of the wavefunction requires not only small transverse but also small longitudinal momentum transfer. This leads to the *coherence condition* (see e.g. [17, 18]):

$$\xi \approx \frac{M_X^2}{s} < \frac{m_\pi}{m_p} \approx 0.1 - 0.2. \tag{10}$$

The upper-limit on M_X, (10), implies that the diffractive hadronic final states exhibit a large rapidity gap between the quasi-elastically scattered proton and the dissociation products X of the projectile. The width of the gap in (pseudo-)rapidity space measured from the rapidity of the initial-state proton is $\Delta\eta \approx \ln\frac{1}{\xi}$. In collider

experiments diffractive events are thus identified either by detecting directly a "fast" (leading) proton in a spectrometer, by the presence in the main detector of a large rapidity region devoid of hadrons (a rapidity gap), or by exploiting the characteristic $1/M_X^2$ dependence of diffraction.

4.2. Hadron hadron inelastic diffraction

Evidence for an important diffractive component in the inclusive reaction $p + p \rightarrow p + X$, with excitation of large masses, was first established at the ISR by the CHLM collaboration [19]. Figure 6 shows single diffractive pp cross sections from low to high s. The diffractive enhancement becomes less and less prominent as s decreases, in line with the previous discussion about the need to maintain coherence of the target. The M_X-spectrum drops rapidly in the resonance region. Beyond that it levels-off and shows an approximite $1/M_X^2$ dependence. A compilation of measurements [20], now plotted against M_X^2, is shown in figure 7 for pp and $\bar{p}p$ single diffractive cross sections at $t = -0.05$ GeV^2 (for earlier compilations see [21]). The distribution falls as $1/(M_X^2)^{1+\Delta}$ over the entire M_X region. Quite remarkably, it is independent of s over five orders of magnitude. The data are consistent with the same value of $\alpha_{I\!P}(0) - 1 = \epsilon = 0.104$ (denoted Δ in the figure) as that extracted from the fit in [7] to total and elastic cross sections data.

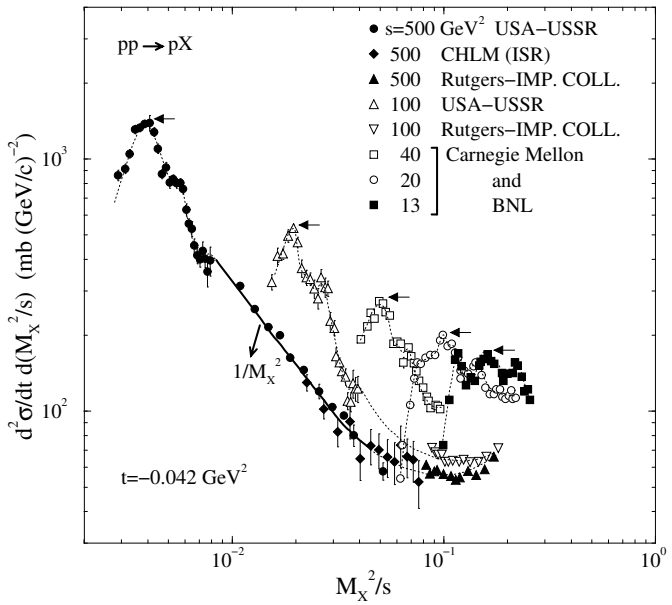

Figure 6. Single diffractive pp cross sections [18]). The figure shows how the characteristic $1/M_X^2$ (Regge) behavior of diffraction becomes manifest as s increases. The arrows indicate the low mass ($M_X \approx 2$ GeV) resonance region. From [30].

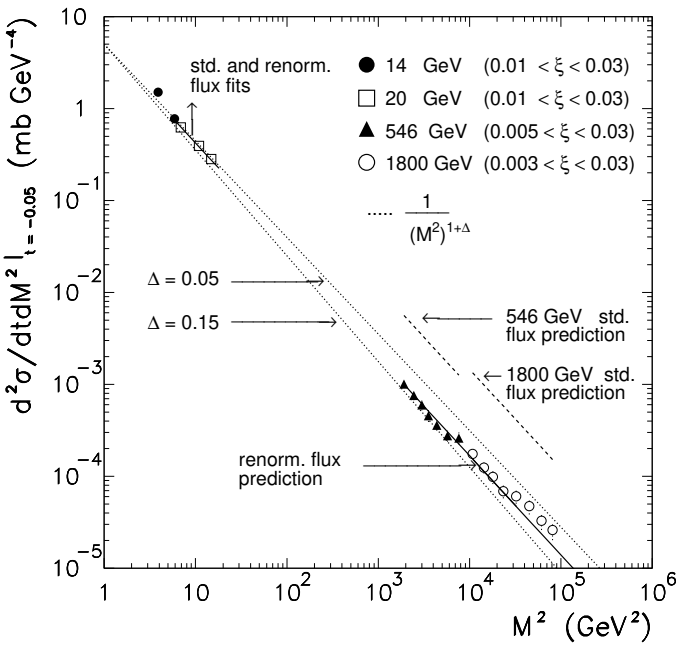

Figure 7. Cross sections $\mathrm{d}^2\sigma_{sd}/\mathrm{d}M_X^2 dt$ for $p + p(\bar{p}) \to p(\bar{p}) + X$ at $t = -0.05$ GeV^2 and $\sqrt{s} = 14, 20, 546$ and 1800 GeV. For a description of the curves see [20].

4.3. Inclusive diffraction at HERA

In DIS at small x at HERA, inelastic diffraction occurs at a rate of $\mathcal{O}(10\%)$ of all events [22]. Although it surprised many in the pQCD community, it had been anticipated even before the advent of QCD [23]. It was also predicted from Regge theory [24]. The occurrence of such diffractive events is difficult to understand in the independent parton picture on the basis of pQCD alone.

The experimental effort at HERA has concentrated on measurements of the diffractive part, $F_2^{D(3)}$, of the structure function F_2, (4). The data have been reviewed at many occasions and details can be found in [1, 2, 25, 10].

New preliminary H1 1997 inclusive diffractive data [26] have been used to extract $\alpha_{I\!P}(0)$ from the ξ-dependence of $F_2^{D(3)}(\beta, Q^2, x_{I\!P})$ with much increased precision, yielding $\alpha_{I\!P}(0) = 1.173 \pm 0.018(\mathrm{stat.}) \pm 0.017(\mathrm{syst.})^{+0.063}_{-0.035}(\mathrm{model})$. This value is not much higher than $\alpha_{I\!P}(0) \simeq 1.1$ in soft processes. As figure 8 shows, their is no evidence for a systematic variation with Q^2. The data suggest that the effective intercept for $\sigma_{\mathrm{T}}(\gamma^\star p)$ grows faster than that of the diffractive contribution at high Q^2.

Another striking HERA result, first obtained by ZEUS [27], is illustrated in figure 9 from H1. This shows that, for Q^2 and M_X (or β) fixed, the relative rate of diffractive events is nearly W-independent, except at very small β. This disagrees with the (standard) triple-Regge expectation which predicts an increase as s^ϵ. As discussed in [28], no adequate explanation within purely pQCD of the constancy of the mentioned ratio is known at present. The authors conclude that the nonperturbative QCD contribution to diffractive production is essential. Indeed, constancy of the ratio follows

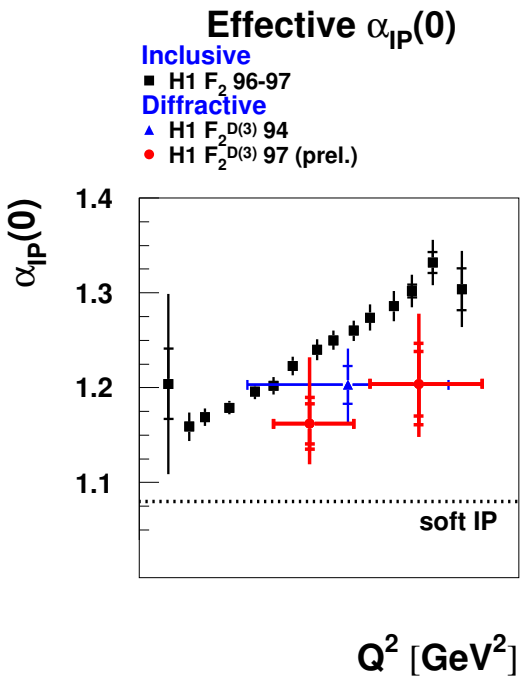

Figure 8. H1: effective value of $\alpha_{I\!P}(0)$ as function of Q^2: ● extracted from $F_2^{D(3)}$; ■ from a fit of $F_2(x, Q^2)$ to the form $x^{-\lambda(Q^2)}$; ▲ H1 1994 data [40]. From [26].

.

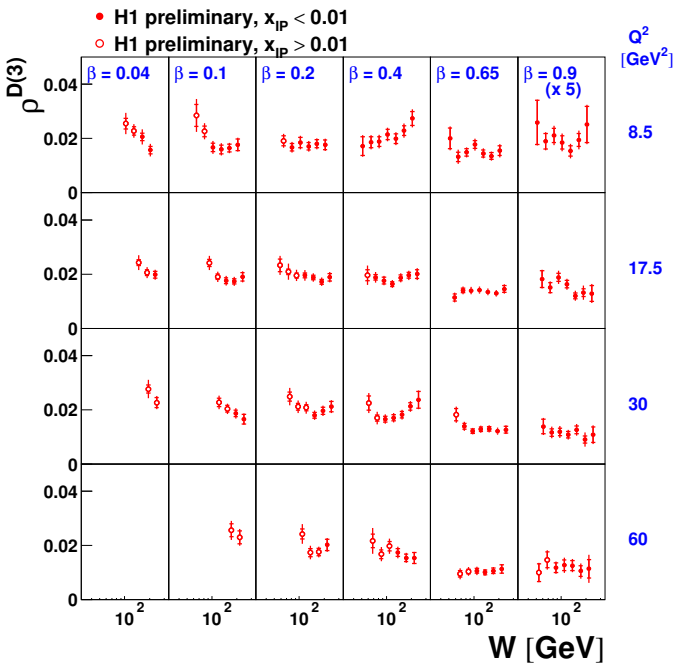

Figure 9. H1-97 measurements of $\rho^{D(3)}$, the ratio of the diffractive to the inclusive cross section versus W. Data points at $\beta = 0.9$ are scaled by a factor of 5 [26].

from the quasi-classical gluon field approach (see Buchmüller in [2]). It is also correctly predicted in the GBW-model [29], where it is a consequence of the basic assumption that the interaction cross section of the system radiated off the $\gamma^\star$ partonic fluctuations saturates once this system has acquired a large transverse extension and is thus non-perturbative.

Whereas diffractive data at very small ξ and so-called Leading-Baryon data at larger ξ, outside of the diffractive region, are usually analyzed separately, a noteworthy exception is that of ref. [30]. There, diffractive structure function measurements have been combined with Leading-Proton and Leading-Neutron data from H1. Results are shown in figure 10 [30] which displays $\xi\, F_2^{LP}$ and $\xi\, F_2^D$ as a function of ξ. A combined fit, including Pomeron-, Reggeon- and pion contributions yields $\alpha_{I\!P}(0) = 1.250 \pm 0.023$ and a Reggeon trajectory compatible with f_2 exchange: $\alpha_{I\!R}(0) = 0.770 \pm 0.030$. Note the somewhat larger value of $\alpha_{I\!P}(0)$ compared to that quoted above.

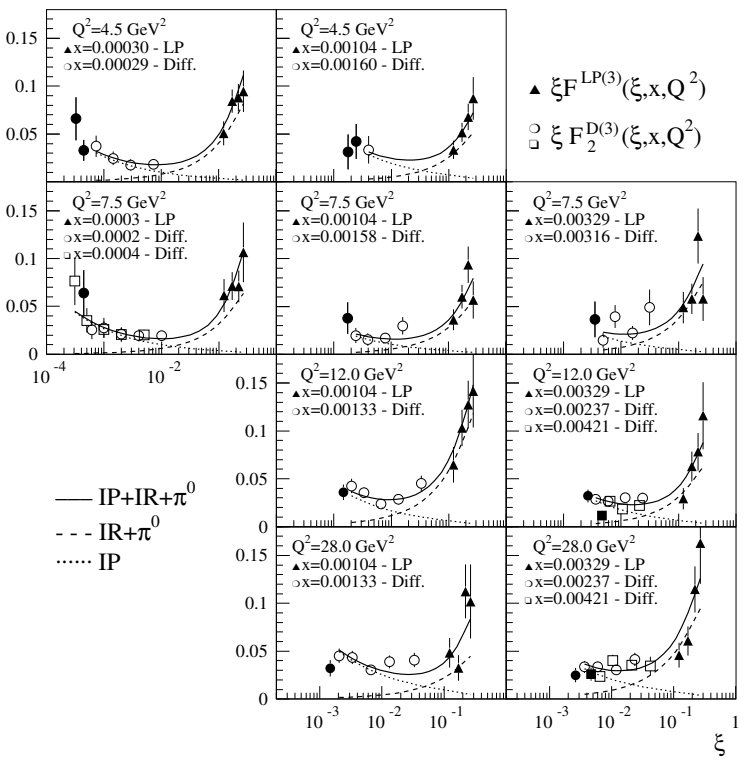

Figure 10. Diffractive (Diff, open circles and open squares) and leading proton (LP, black triangles) structure function data vs. ξ, for fixed x and Q^2. The figure combines, in each plot, the diffractive and leading proton H1 data with similar values of x and Q^2. The quoted Q^2 values are those of the diffractive data; the corresponding Leading Proton values are $Q^2 = 4.4,\ 7.5,\ 13.3$ and 28.6 GeV^2. The black circles and black squares are data with $M_X < 2$ GeV. The plotted curves represent a global fit: total (solid line), pomeron (dotted line) and reggeo n plus pion contributions (dashed line). For details ands references see [30].

5. Unitarity

The importance of unitarity is, especially among (young) experimentalists, not always sufficiently appreciated. This section is therefore devoted to a description of its main aspects and implications.

The unitarity of the scattering matrix, T, implies close relationships between total cross sections, the elastic scattering amplitude and the amplitudes of inelastic final states. The unitarity relation between states $|i>$ and $|f>$ reads

$$2\text{Im } <f|T|i>= \sum_{|e><e|} <f|T^+|e><e|T|i> + \sum_{|n><n|} <f|T^+|n><n|T|i>, \tag{11}$$

where $\sum_{|e><e|}$ stands for summation and integration over all possible *elastic* intermediate states $|e>$. The second term is the contribution from all possible inelastic states; $|i>$ is the initial and $|f>$ an *arbitrary* final state.

For forward elastic scattering, $t = 0$, ($|i> \equiv |f>$) (11) immediately leads to the optical theorem. However, the relation has much wider consequences since the state $|f>$ can be any state. It shows that the imaginary part of the amplitude of any particular final state $<f|T|i>$ in general receives contributions from all other final states. Such "unitarization effects" will be small only if the "overlap" ($<f|T|n><n|T|i>$) of the states $|i>, |f>$ with the states $|n>$ happens to be small. This will, therefore, depend crucially on the topology in momentum space of the inelastic states and on the phases of the amplitudes.

The two terms at the right-hand side of (11) are called the elastic and inelastic overlap functions, respectively, and were first introduced by Van Hove [31]. For elastic scattering (and neglecting the real part), the amplitude can, in principle, be calculated from the knowledge of the inelastic final states. This is the so-called s-channel approach to diffractive scattering. An important result is obtained (valid only at high s) when (11) is written in impact-parameter ($\vec{b}$) space. Using angular momentum conservation one finds

$$2\,\text{Im } \mathcal{A}_{el}(s,b) = |\mathcal{A}_{el}(s,b)|^2 + G_{in}(s,b). \tag{12}$$

Here $\mathcal{A}_{el}(s,b)$ is the elastic amplitude; $G_{in}(s,b)$, the inelastic overlap function, is the contribution from all inelastic channels. From (12) follows that Im $\mathcal{A}_{el}(s,b)$ at impact parameter b is generated by the absorption into the inelastic channels *at the same* impact parameter: "unitarity is diagonal in b-space".

For $\text{Re}\,\mathcal{A}_{el} = 0$, (12) can be solved easily for $\mathcal{A}_{el}$ if $G_{in}(s,b)$ is known. Alternatively, knowledge of $\mathcal{A}_{el}(s,b,t)$ can be used to determine $G_{in}(s,b)$ (see e.g. [8]). For DIS, it is presently unknown but of great interest. For a recent exploratory analysis see [32].

5.1. Elastic diffraction and shrinkage

The physical meaning of the elastic forward slope $B(s)$ can be understood from the shape of $G_{in}(s,t)$ and follows directly from (11). The inelastic overlap function measures the overlap of the amplitude of a given inelastic final state with *the same* state but rotated

along the incident direction over an angle θ, the scattering angle. For a large majority of the final states $|n>$, the transverse momentum of produced particles, p_T, relative to the incident direction is sharply cut off, and $\langle p_T^2 \rangle$ increases slowly with s: the distribution in rapidity-p_T space resembles that of a uniformly filled cylinder, sometimes called a "Wilson-Feynman liquid", with short-range correlations only between the hadrons. For such a configuration, it is easily verified that the inelastic overlap function, and thus $\mathrm{Im}\,\mathcal{A}_{el}$, will fall-off exponentially with t, at small $|t|$, with a slope determined by the mean number of particles produced and by $\langle p_T^2 \rangle$. For example, in a model of uncorrelated particle production, one finds [31] (see also [33])

$$B(s) \geq \text{constant} + \langle n \rangle / \langle p_T^2 \rangle. \tag{13}$$

Consequently, $B(s)$ grows with energy like $\langle n \rangle$, *the mean multiplicity of produced hadrons* provided that $\langle p_T^2 \rangle$ is constant. This explains qualitatively the origin of the shrinkage of $\mathrm{d}\sigma_{el}/\mathrm{d}t$. Writing $\langle n \rangle = \omega_0\, \Delta y = \omega_0 \ln(s/s_0)$, $B(s)$ is seen to depend on the particle density in rapidity space in *inelastic collisions* and on $\langle p_T^2 \rangle$. In a more rigorous approach, the second-order *transverse momentum transfer* correlation function replaces $\langle p_T^2 \rangle$ in (13) [34]. In pQCD "ladder-language", this corresponds to the correlation function between adjacent propagator transverse momenta which should be calculable. The link between gluon correlators and $\alpha'_{I\!P}$ has been studied in [35].

The result (13) is generic [36]. For inelastic final states where $\langle p_T^2 \rangle$ is larger than a soft scale, or large compared to $|t|$, the second term at the right-hand side of (13) will be less important and shrinkage will either be small or absent. This most likely happens in (quasi-)elastic processes, such as $\gamma^\star p \to \mathrm{J}/\Psi\, p$, where a large scale can be identified. These are often referred to as "hard diffraction".

In a general collision process, and for $\gamma^\star p \to X$ in particular, both ω_0 and $\langle p_T^2 \rangle$ can be expected to be process- and (perhaps) energy-dependent. There is no reason to believe that these quantities, and thus the intercept and slope of the dominant trajectory in the t-channel Regge formalism, are universal.

The above should suffice as an illustration of the deep connection between global properties of the *inelastic final states*, diffractive scattering and Regge trajectory parameters. Since the important dynamical ingredients, here ω_0, $\langle p_T^2 \rangle$, are clearly identified, generalization beyond the Regge framework is, at least conceptually, simple to understand.

5.2. Inelastic diffraction as a regeneration process

The possibility of inelastic diffraction has been predicted in the seminal papers by Feinberg and Good and Walker [16]. Assume that the projectile, $|B>$, at a fixed impact parameter ($\vec{b}$) from the target is a linear combination of states which are eigenstates of diffraction

$$|B\rangle = \sum_k C_k\, |\Psi_k\rangle\,, \tag{14}$$

$$\mathrm{Im}T\, |\Psi_k\rangle = t_k\, |\Psi_k\rangle\,; \tag{15}$$

where ImT is the imaginary part of the scattering operator and the (real) eigenvalue t_k is the probability for the state $|\Psi_k\rangle$ to interact with the target. The absorption coefficients t_k, of course, vary with $\vec{b}$. The states are normalized so that $< B|B >= \sum_k |C_k|^2 = 1$. From (14) and (15) one easily derives

$$\mathrm{d}\sigma_{\mathrm{T}}/\mathrm{d}^2b = 2\,\langle t\rangle, \tag{16}$$

$$\mathrm{d}\sigma_{\mathrm{el}}/\mathrm{d}^2b = \langle t\rangle^2. \tag{17}$$

The cross section for diffractive production, with elastic scattering removed is

$$\mathrm{d}\sigma^{\mathrm{DD}}/\mathrm{d}^2b = \langle t^2\rangle - \langle t\rangle^2. \tag{18}$$

The brackets $< \cdots >$ denote an average of t_k or t_k^2, weighted according to their probability of occurrence, $|C_k|^2$, in $|B\rangle$. Inelastic diffraction is seen to be proportional to the variance in cross sections of the diagonal channels.

From (18) follows that, contrary to elastic scattering, inelastic diffraction will be strongest in regions of b-space where absorption shows the strongest *variation* i.e. at the "edges" of the target: hadronic inelastic diffraction is more peripheral than the elastic process which is largest at small b [8]. In the case of complete absorption at a given b, inelastic diffraction vanishes at the same b.

Note that for virtual photon scattering, the purely elastic reaction can be neglected. In this case, the term $< t >^2$ in (18) is absent. The impact parameter profile for DDIS may therefore be more central (smaller b) than that of hadronic inelastic diffraction and thus more sensitive to saturation effects. Experimentally very little is known about the impact parameter profile. For this a measurement of the t-dependence over a wide t-range is needed. For elastic ρ production it was studied for the first time in [32], following the method of Amaldi and Schubert [8].

As remarked in [37], "The increase of σ_{T} with energy occurs because some regions of impact parameter are changing from grey to black and regions at larger b are going from white (no absorption) to grey. However, the region where absorption shows the strongest variation, and which contributes to diffraction, grows less rapidly than those b-regions giving elastic and highly inelastic scattering. This would explain the observation that the inclusive diffractive cross section grows less rapidly than expected from Regge arguments (cfr. figure 9). Regge theory is indeed expected to hold for those regions in b where the absorption is weak. Regions of large absorption then correspond to multiple Pomeron exchanges."

6. A generic picture of high energy collisions

Well before the advent of QCD, and inspired by the ideas of Ioffe, Feinberg, Gribov, Pomeranchuck and others, a basic understanding of the space-time evolution of a high-energy scattering process was developed [23, 38, 39]. It testifies to the profoundness of these ideas that, in spite of major advances in the field of strong interactions, the physical picture then developed still remains largely valid. Perturbative QCD has allowed to clarify many issues, and produce crisp quantitative predictions in some cases, but the

ideas then formulated, reaching well beyond pQCD, continue to be of great value. They provide a view of the collision dynamics which greatly aids in developing intuition, provide physical insight and, hopefully, inspire new directions for theoretically unbiased experimental research.

6.1. The Gribov-Feynman parton model

The parton model views a high-energy interaction of any projectile, particle 1, with a target, particle 2 *at rest* as follows (see figure 11). The fast projectile fluctuates into point-like partons: quarks and gluons. The fluctuations have a lifetime $t \propto \frac{E}{\mu^2}$ before interaction with the target occurs; E is the projectile's energy and μ is a *transverse mass* scale. Each parton can, in turn, create its own parton cascade, each creating $\langle n \rangle$ partons, resulting eventually in the emission of a total of N soft partons (*"wee" partons* in Feynman's terminology [38]). The latter should not be confused with the partons of pQCD. They are non-perturbative ("dressed") objects due to the long time-evolution of the cascade and have acquired a large transverse extension. They interact with the target with a large hadron-like cross section.

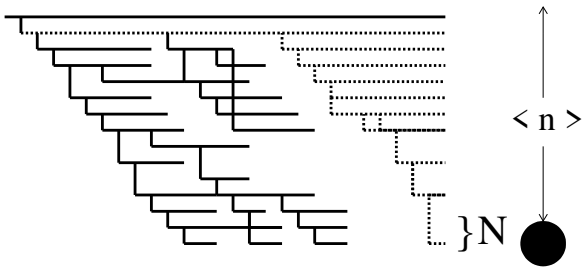

Figure 11. A high energy interaction in the parton model. From [36].

.

For a highly virtual photon in DIS, the cascade starts with a $q\bar{q}$ fluctuation (or dipole) of small transverse extension and is followed by an initial evolution stage where the strong coupling remains perturbative and the process calculable. However, the non-perturbative end of the cascade is likely to be similar to that originating from a high-energy hadron. Since gluons rather than quarks will be the dominant soft component of the cascade, and since gluons carry a larger color charge, it is evident that the interaction, when viewed in an infinite-momentum frame, will be driven by the gluon constituents in the proton. The same applies to "diffractive" structure functions of the proton or of the Pomeron.

As argued by Gribov [39], a fast projectile can interact with the target only through its wee component. Indeed, the cross section of interaction of two point-like particles with large relative energy, $\sqrt{s}_{ab}$, is not larger than $\pi\lambda^2 \sim 1/s_{ab} \sim \exp(-\eta_{ab})$ (λ is the wavelength in the c.m. frame of a, b, η_{ab} is the relative rapidity). Thus, *only slow partons of the projectile* are able to interact with a non-negligible cross section. Since there are

N wee partons in total, the interaction cross section is proportional to the probability that *at least one* wee parton out of N interacts with the target. If the interaction probability is f, the inelastic cross section will be proportional to $1-(1-f)^N$; for small Nf this is proportional to $N\,f\|$.

The interaction can also be viewed from the rest-frame of the projectile, or from any collinear rest-frame. The distribution of the wee partons in the rest-frame of particle 2 is, according to the above arguments, solely determined by particle 1 and does not depend on the properties of particle 2. On the other hand, in the rest frame of particle 1 the distribution is determined by the properties of particle 2. This is possible only if the distribution of partons with rapidities η much smaller than the target and projectile's rapidity, η_p, *does not* depend on the quantum numbers and the mass of that hadron. It follows that *the distribution of the wee partons with $\eta \ll \eta_p$ should be independent of the projectile and target*, i.e. be "universal".

The "universality" of the wee-parton distribution explains why hadronic total cross sections show a "universal" energy-dependence at large s, as discussed in section 3.1. In addition, if the interaction between wee's is effectively short-range in rapidity (implying that the produced hadrons show short-range rapidity correlations), hadrons produced in regions of rapidity sufficiently far from target and projectile will also show "universal" properties. This explains much of the phenomenology of particle production in the central and target/projectile fragmentation regions.

6.1.1. Shrinkage. Consider the parton cascade in figure 11. In each step the newly emitted parton acquires a random amount of transverse momentum, k_T. The last parton in the cascade will thus have moved a distance b_N^2 from the origin in impact-parameter space. On average, and for a purely random walk (*which precludes any kind p_T-ordering of the emissions*), one has

$$\langle b_N^2\rangle \propto \frac{1}{\langle k_T^2\rangle}\,N = \frac{\omega_0}{\langle k_T^2\rangle}\,\ln s/s_0, \tag{19}$$

for $N \propto \ln s$. The region occupied by wee partons grows with energy and $\omega_0/\langle k_T^2\rangle$ can be identified with $\alpha'_{I\!P}$. The argument based on the overlap function, section 5.1, leads to the same result but is more general.

It is superfluous to mention that wee-parton properties, and their interactions, cannot be calculated in pQCD, neither for hadronic collisions nor for deep-inelastic ep scattering, since they are associated with long-wavelength fluctuations of the colour fields. For DIS, this ignorance is parameterized in the parton distributions at a small Q^2 scale. However, for large $1/x$ *the wee partons are equally important in both types of scattering process*. Progress can be made if the colour fields are strong enough so that semi-classical methods can be employed. The so-called Color Glass Condensate method, based on stochastic Yang-Mills theory, has recently lead to remarkable advances,

‖ For large $N\,f$, the whole multiple-scattering series must be considered, as well as parton-parton correlations.

including a calculation of gluon saturation, and fascinating new insights. They are reviewed in [41].

6.1.2. Rise of the total cross section and $\alpha_{I\!P}(0)$. Consider again figure 11. Since each parton in the parton cascade can form its own chain of partons, and so on, this multiplication process will generically (but not in detail) lead to a total mean $N \sim e^{\langle n \rangle}$, if $\langle n \rangle$ is mean multiplicity in a single chain. With $\langle n \rangle \propto \omega_0 \ln s$ one finds, in a frame-independent form [36]

$$\sigma_{\rm T} = \sigma_0(\text{projectile}) \times \sigma_0(\text{target}) \times \frac{1}{s_0} \times \left(\frac{s}{s_0}\right)^{\omega_0}. \tag{20}$$

The "impact-factors", σ_0, are particle-specific but independent of s. Equation (20) "explains" the power-law (or Regge) behaviour of $\sigma_{\rm T}$.

We see again that $\alpha_{I\!P}(0) - 1$ in Regge theory has the physical meaning of a wee-parton density in a parton cascade. This result is generic. However, since the detailed process-specific dynamical evolution of the cascade (DGLAP [42], BFKL [43],...) will influence the value and evolution of ω_0, we conclude that a "universal" Pomeron trajectory with process-independent parameters does not exist.

6.2. Models for diffraction

6.2.1. The Miettinen and Pumplin paper. The first detailed calculations of hadronic diffraction in the framework of the parton model were presented in [44]. This work, although 22 years old and not too well known, remains of great interest and we summarize its main conclusions.

It is assumed that the diagonal states (section 5.2), $|\Psi_k>$, are the states of the parton model, composed of quarks and gluons and a radiation cloud of wee partons. These states are characterized by a certain number N of partons with relative impact parameters $\vec{b}_1, \ldots, \vec{b}_N$ and rapidities, $y_1, \ldots, y_N$. These states will interact with a target with very different cross sections. Hence, inelastic diffractive will be generated by the mechanism of Good and Walker. Assuming uncorrelated wee partons, and fitting all free parameters of the model to $\sigma_{\rm el}(pp)$ and $\sigma_{\rm T}(pp)$ at $\sqrt{s} = 53$ GeV, the calculated total inelastic diffractive cross section was found to be in very good agreement with data. The y_i fluctuations contribute little (about 10%), whereas fluctuations in b_i and in parton number each account for about 45% of $\sigma_{\rm in}^{\rm DD}$. Also the forward value and the slope t-distribution of inelastic diffraction are correctly predicted. This is non-trivial since the calculated (and measured) slope $B \approx 6.9$ GeV^{-2} is only about half that of elastic scattering $B \approx 12$ GeV^{-2}. Interestingly, small $|t|$ dissociation turns out to be *dominated* by the large and very steep (slope ≈ 12.2 GeV^{-2}) contribution due to the *parton-number fluctuations*. The b_i fluctuations, on the other hand, dominate at large $|t|$, see figure 5 in [44].

The ZEUS collaboration recently presented new measurements [45] of the t-slope in diffractive DIS, using their Leading Proton Spectrometer (LPS). The slope has a value

$B = 6.8 \pm 0.6\,(\mathrm{stat})^{+1.2}_{-0.7}\,(\mathrm{syst})$ for $4 < Q^2 < 100$ GeV^2, $M_X > 2$ GeV, $\xi < 0.03$. Some evidence for shrinkage is seen but no dependence on Q^2. These results are in perfect agreement with hadron data and are consistent with the hadron-like character of DDIS.

6.3. Modern QCD models of diffraction

It is evident that the Miettinen-Pumplin (MP) model grasps the essential physics which remains valid in the context of DDIS at HERA. In [44] ad-hoc assumptions were needed to build a model of the hadron Fock states. In DIS the lowest-order Fock states $\gamma^\star$ fluctuations are calculable in pQCD [23, 46] and quantitative results can be obtained. Nevertheless, the interaction of the wee partons needs to be parameterized empirically, as it must be for soft hadron-hadron collisions.

The present popular DDIS models have been widely discussed at this Workshop and we can be brief. For reviews see [2]. The models use the same basic concepts discussed in previous sections under various disguises. The most successful of these are merely modernized versions of the Aligned Jet Model [23] which predates QCD.

Consider, as an example, the very successful saturation model of Golec-Biernat and Wüsthoff (GBW) [29] which expands on much earlier ideas [46]. The physical picture is that in which, in the nucleon rest frame, a photon with virtuality Q^2, emitted by a lepton, dissociates into a $q\bar{q}$ pair far upstream of the nucleon. This is then followed by the scattering of the colour dipole on the nucleon. In this picture the relative transverse separation ϱ of the $q\bar{q}$ pair and the longitudinal photon momentum fraction z of the quark are "good" degrees of freedom, as also assumed in the MP model. The $\gamma^\star p$ cross sections take the following *factorized* form [46, 47]

$$\sigma_{T,L}(x,Q^2) \;=\; \int \mathrm{d}^{\,2}\varrho \int_0^1 \mathrm{d}z\, |\Psi_{T,L}\,(z,\varrho)|^2\, \sigma\,(x,\varrho^2), \tag{21}$$

where $\Psi_{T,L}$ is photon wave function of transversely (T) and longitudinally polarized (L) photons.

In (21), all Q^2 dependence is contained in the Fock-state wavefunction, which further depends on the flavour and mass of the partons. The W- or x-dependence of $\sigma_{T,L}(x,Q^2)$ is solely determined by that of $\sigma\,(x,\varrho^2)$. Once the dipole cross section is known, (21) enables a parameter-free calculation of the proton structure function at small x. In our simple picture, we may interpret it as an effective cross section, the product of the wee-parton flux with the single wee-parton nucleon cross section. The latter is assumed to be universal, in accord with the Gribov-Feynman argument of wee-parton scattering and should be nearly energy-independent. Although the impact-parameter dependence of $\sigma\,(x,\varrho^2)$ is not explicitly considered, (in (21) only its average enters), this is clearly of great interest for the t-dependence of the diffraction [32].

Turning to diffraction, the differential cross section at $t = 0$ takes the form

$$\left.\frac{\mathrm{d}\sigma^D_{T,L}}{\mathrm{d}t}\right|_{t=0} \;=\; \frac{1}{16\pi}\; \int d^{\,2}\varrho \int_0^1 \mathrm{d}z\, |\Psi_{T,L}\,(z,\varrho)|^2\, \sigma^2\,(x,\varrho^2). \tag{22}$$

The structure of (22) differs only from (21) by the substitution $\sigma(x,\varrho) \rightarrow \sigma^2(x,\varrho)$, in accord with the general formula, (18)¶. Comparing to the MP-model, we see that the relative impact parameter and rapidity fluctuations are included here through the photon wave function. The important parton-number fluctuations, which also depend on parton-parton correlations however, are not explicitly considered.

The energy-dependence of $\sigma\,(x,\varrho^2)$ follows from the fact that, in low-x DIS, the perturbative evolution of the $q\bar{q}$ results in further "hard" parton multiplication which increases also the wee-parton flux and thus the total cross section. Indeed, due to the bremsstrahlung spectrum of soft gluons $\propto \mathrm{d}z_g/z_g$ (z_g is the momentum fraction of the photon carried by a gluon) Fock states with n such gluons give a contribution $\propto \ln(1/x)^n$ to the total photoabsorption cross section, which can be reabsorbed into an energy-dependent dipole cross section [46]. For example, in the DGLAP regime, summing over all n produces the well-known $\exp\left[2\sqrt{\ln(1/x)\ln\left(1/\alpha_s(Q^2)\right)}\right]$ increase of the $\gamma^\star p$ cross section and "standard" scaling violations.

The $q\bar{q}$ dipole-proton cross section $\sigma(x,\varrho^2)$ has to be modelled although it is known in the perturbative limit of very small dipoles and related there to the inclusive gluon distribution $xg(x,\mu^2)$ of the target [48]. For a $(q\bar{q}g)$-dipole system, $\sigma(x,\varrho^2)$ is roughly a factor 9/4 larger. This explains the predominant role of gluons in low-x DIS. In the GBW model, the effective dipole cross section has the form

$$\sigma(x,\varrho^2) \;=\; \sigma_0\,\left[1\,-\,\exp\left(-\frac{\varrho^2}{4R_0^2(x)}\right)\right], \tag{23}$$

where the x-dependent radius R_0 is taken to be $R_0(x) = (1/Q_0)\;(x/x_0)^{\lambda/2}$; $Q_0 = 1$ GeV. $\sigma_0 = 23$ mb, $x_0 = 3\,.\,10^{-4}$ and $\lambda = 0.29$ have been determined by a fit to data on F_2 [29]. The dipole cross section saturates at a value σ_0 for large-size dipoles where it is entirely non-perturbative. Also, as $x \rightarrow 0$, saturation sets in for decreasing transverse sizes.

Since (22) contains $\sigma^2(x,\varrho^2)$, it follows that larger sizes are involved in diffraction than those dominating the total cross section: non-perturbative soft physics is of even greater importance in DDIS. Saturation effects following from parton recombination can therefore be expected to be larger than in inclusive DIS. Because of the saturation property of (23), nearly the same dependence on x and Q^2 of DDIS and DIS is found, thus giving a natural explanation of the constancy of their ratio, discussed in section 4.3.

In the GBW model, two essential scales appear: the characteristic transverse size of the $q\bar{q}$ dipole $\propto 1/Q$, solely determined by the $\gamma^\star$ wave function, and $R_0(x)$. $1/R_0^2(x)$ can be interpreted as the *mean number of wee partons* in the cascade; $R_0(x)$ is their mean relative transverse distance and $Q\,R_0(x) = 1$ defines a critical line. For $1/Q \ll R_0(x)$ the partonic system is dilute, for $1/Q \gg R_0(x)$ the system is densely packed and multiple scattering and parton-interactions become important. The quantity

¶ In the dipole formulation of DIS, and contrary to hadron diffraction, even inelastic DDIS is considered to be purely elastic: the dipole states $(q\bar{q})$ and higher-order Fock-states $q\bar{q}$ + gluons are assumed to be orthogonal eigenstates of the diffractive T-matrix, and no regeneration (mixing of the states) occurs. I am not sure how valid this assumption is.

$1/\tau = (1/Q^2)\,(1/R_0^2)$ is proportional to the total number of partons able to interact with the target. One can therefore expect that the total cross section will depend on τ and not on Q^2 and R_0^2 separately, i.e. exhibit "geometrical scaling" [49]. This follows already from dimensional arguments but also agrees with the "universality" hypothesis, advanced in [50], that the physics should depend only on the number of partons per unit of rapidity and per unit of transverse area.

Interestingly, the parameter λ, which can be interpreted as a parton rapidity-density, is quite close to that derived from the c.m. energy-dependence ($\sqrt{s}$) of the mean particle multiplicity in e^+e^- annihilation, where $< n > \sim s^{0.25}$ provides a reasonable fit of the data [51]. The diffractive structure function has a Regge-like factorization property (except for $\beta \to 1$ where higher-twist contribution from longitudinal photons dominate) with the dependence $F_2^D \propto (1/\xi)^{1+\lambda}$, leading to an effective Pomeron intercept $\alpha_{I\!P}(0) \sim 1 + \lambda/2$ [52]. This is a highly revealing result, demonstrating, on this specific model-example, the generic property that both the growth of the cross sections with energy and the proton energy-loss spectrum (or "Pomeron flux") are determined by the density of wee partons, as argued earlier.

From an experimental point of view, high-parton density effects should me most important in diffractive events with large final-state multiplicity. Given the present interest in this topic, a dedicated measurement of the W, Q^2-dependence of total and diffractive cross sections for such events should be of considerable interest[+].

Further properties of the $\gamma^\star$ Fock states allow to understand much of the phenomenology of diffraction. We mention only a few.

• The M_X distribution for the lowest-order $q\bar{q}$ dipole state, and transversely polarized $\gamma^\star$, has the form $1/[m_f^2(Q^2+M_X^2)^2]$ (m_f is the quark mass). Extra soft gluon emission, with a spectrum $\mathrm{d}z_g/z_g$ directly leads to the much weaker M_X dependence $\mathrm{d}M_X^2/(M_X^2+Q^2)$ in the so-called triple-Pomeron region [46]. Since the invariant mass of the diffractive system will remain almost unchanged for small-t scattering, this is also the distribution of the experimentally measured M_X. A similar argument was used in [53] to explain the $1/M_X^2$ dependence of hadronic diffraction at large M_X. The gradual transition from a steep $1/M_X^4$ to a $1/M_X^2$ dependence is a consequence of a change in the mixture of Fock states as Q^2 and/or W change.

• The average transverse size of $\gamma^\star$ fluctuations relevant for elastic vector meson production, the so-called scanning radius [15], is estimated to be $\sim C/(m_V^2 + Q^2)$, with $C \sim 2$ ($C \sim 6$) for longitudinally (transversely) polarized $\gamma^\star$ [32]. This follows almost directly from the form of $|\Psi_{T,L}|^2$. The elastic vector meson data (see e.g. figure 5 in section 3.3.2) show that scale $Q_0^2 = Q^2 + m_V^2$ is indeed the dynamically relevant observable. For further discussion on this point we refer to [10].

The model results, discussed previously in the target rest frame, can be translated, at least in leading twist, in terms of diffractive parton densities (DPD) in an infinite momentum frame. The diffractive structure functions are then expressed as the

[+] I wish to thank A. Białas for pointing this out.

convolution of "diffractive" parton densities *for the proton* with parton cross sections. Their evolution with Q^2 at fixed x is the same as that of $F_2(x, Q^2)$. In DDIS, these scaling violations affects the β (or M_X) dependence of the cross section but not the dependence on ξ. However, unlike inclusive scattering, the DPD's are no longer universal, and of little direct use in hadronic interactions [52].

Acknowledgments

It is a pleasure to thank the organisers of the Ringberg Workshop on "New Trends in HERA Physics 2001" for a very stimulating meeting in a splendid environment. I also thank A. Białas for interesting discussions and A. De Roeck and G. Lafferty for reading of the manuscript and helpful comments.

References

[1] Abramowicz H, Caldwell A, *Rev. Mod. Phys.* **71** (1999) 1275; Abramowicz H, *Int. J. Mod.Phys.* **A15S1** (2000) 495; eConf C990809 (2000) 495.
[2] Wüsthoff M and Martin A D, *J. Phys.* G **25** (1999) R309 [hep-ph/9909362]; Hebecker A, *Acta Phys. Pol.* B **30** (1999) 3777; *Phys. Rep.* **331** (2000); Buchmüller W, *Towards the theory of diffractive DIS*, talk presented at "New Trends in HERA Physics", Ringberg Workshop, 1999 [hep-ph/9906546]; Hebecker A, *Phys. Rep.* **331** (2000) 1 [hep-ph/9905226].
[3] Ingelman G and Schlein P, *Phys. Lett.* B **152** 1985 256.
[4] Donnachie A and Landshoff P V, *Nucl. Phys.* B **231** (1984) 189.
[5] Donnachie A and Landshoff P V, *Phys. Lett.* B **296** (1992) 227.
[6] Cudell J R *et al* , *Soft pomeron and lower-trajectory intercepts* [hep-ph/9812429]; Kang K *et al* , *Analytic amplitude models for forward scattering* [hep-ph/0111360].
[7] Covolan R, Montanha J and Goulianos K, *Phys. Lett.* B **389** (1996) 176.
[8] Miettinen H G, in Proc. of the IX th Rencontre de Moriond, Meribel les Allues, Vol. **1** (ed. J. Tran Thanh Van), Orsay (1974); Amaldi U and Schubert K R, *Nucl. Phys.* B **166** (1980) 301.
[9] Clerbaux B, *Vector meson production at HERA* [hep-ph/9908519].
[10] Iacobucci G, *Diffractive phenomena* [hep-ex/0111079].
[11] ZEUS Collab., Abstract 594, EPS2001, July 2001, Budapest, Hungary.
[12] Bartels J and Kowalski H, *Eur. Phys. J.* C **19** (2001) 93 [hep-ph/0010345].
[13] Mellado B, *Vector meson cross sections and trajectory determination*, Proc. Int. Europhysics Conf. on HEP, Budapest 2001.
[14] Nikolaev N N, Zakharov B G and Zoller V R, *Phys. Lett.* B **366** (1996) 337.
[15] Nemchik J, Nikolaev N N and Zakharov B G, *Phys. Lett.* B **341** (1994) 228.
[16] Feinberg E L, *JETP* **29** (1955) 115; Akieser A I and Sitenko A G, *JETP* **32** (1957) 744; Good M L and Walker W D, *Phys. Rev.* D **120** (1960) 1857.
[17] Amaldi U, Jacob M and Matthiae G, *Ann. Rev. Nucl. Sci.* **26** (1976) 385.
[18] Kaidalov A, *Phys. Rep.* **50** (1979) 157; Goulianos K, *Phys. Rep.* **101** (1983) 169.
[19] Albrow M G *et al* , *Nucl. Phys.* B **51** (1973) 388; **72** (1974) 376.
[20] Goulianos K and Montanha J, *Phys. Rev.* D **59** (1999) 114017.
[21] Melissinos A C and Olsen S C, *Phys. Rep.* **17** (1975) 77.
[22] ZEUS Collab., Derrick M *et al* , *Phys. Lett.* B **315** (1993) 481; H1 Collab., Ahmed T *et al* , *Nucl. Phys.* B **429** (1994) 477.
[23] Bjorken J D, AIP Conf. Proc. No.6, eds. M. Bander *et al* (AIP, New York, 1972) p. 151; Bjorken J D, Kogut J B and Soper D E, *Phys. Rev.* D **3** (1971) 1382; Bjorken J D and Kogut J B, *Phys. Rev.* D **8** (1973) 1341.

[24] Donnachie A and Landshoff P V, *Phys. Lett.* B **191** (1987) 309.
[25] Monaco V, *Diffractive structure functions* [hep-ex/0106007].
[26] H1 Collab., *Measurement of diffractive structure function* $F_2^{D(3)}$ *at HERA*, EPS2001, abstract 808.
[27] ZEUS collab., Breitweg J *et al* , *Eur. Phys. J.* C **6** (1999) 43.
[28] Gotsman E *et al* , *Energy dependence of* σ^{DD}/σ_{tot} *in DIS* [hep-ph/0007261].
[29] Golec-Biernat K and Wüsthoff M, *Phys. Rev.* D **59** (1999) 014017, **60** (1999) 114023.
[30] Batista M, Covolan R and Montanha J, *Regge analysis of diffractive and Leading Baryon structure sunctions from DIS* [hep-ph/0006118].
[31] Van Hove L, *Phys. Lett.* **7** (1963) 69, Nuovo Cim. **28** (1963) 798, *Rev. Mod. Phys.* **36** (1964) 655.
[32] Munier S, Stasto A M and Mueller A H, *Nucl. Phys.* B **603** (2001) 427.
[33] Andersson B, *The Lund Model*, Cambridge, Cambridge University Press, 1998.
[34] Krzywicki A, *Nucl. Phys.* B **86** (1975) 296; Grassberger P *et al* , *Nucl. Phys.* B **89** (1975) 101.
[35] Nikolaev N N, Zakharov B G and Zoller V R, *JETP Lett.* **60** (1994) 694.
[36] Levin E, *An Introduction to pomerons* [hep-ph/9808486] and [hep-ph/9710546].
[37] Mueller A H, *Small-x physics and parton saturation in QCD* [hep-ph/9911289].
[38] Feynman R P, *Photon-hadron interactions*, W.A. Benjamin Inc., 1972.
[39] Gribov V N, in: *Materials of the 8th Winter School of the Leningrad Institute of Nuclear Physics 1973* (in russian); [hep-ph/0006158] (english translation).
[40] H1 Collab., Adloff C *et al* , *Z. Phys.* C **76** (1997) 613.
[41] McLerran L, *The color glass condensate and small-x physics* [hep-ph/0104285]; Iancu E, *Gluon saturation at small x* [hep-ph/0111400].
[42] Dokshitzer Yu L, *JETP* **73** (1977) 1216; Gribov V N and Lipatov L N, *Sov. J. Nucl. Phys.* **15** (1972) 78; Altarelli G and G. Parisi G, *Nucl. Phys.* B **126** (1997) 298.
[43] Lipatov L N, *Sov. J. Nucl. Phys.* **23** (1976) 338; Fadin V S, Kuraev E A and Lipatov L N, *Phys. Lett.* B **60** (1975) 50; *Sov. Phys. JETP* **44** (1976) 443, **45** (1977) 199; Balitski Y Y and Lipatov L N, *Sov. J. Nucl. Phys.* **28** (1978) 822.
[44] Miettinen H and Pumplin J, *Phys. Rev.* D **18** (1978) 1696.
[45] Smalska B, *Diffractive results from the ZEUS LPS at HERA*, talk at DIS2001, Bologna.
[46] Nikolaev N N and Zakharov B G, *Z. Phys.* C **49** (1990) 607; **64** (1994) 631 [hep-ph/9306230].
[47] Forshaw J R and Ross D A, *QCD and the pomeron*, Cambridge University Press, 1996.
[48] Frankfurt L, Miller G A and Strikman M, *Phys. Lett.* B **304** (1993) 1 [hep-ph/9305228].
[49] Staśto A M, Golec-Biernat K and Kwieciński J *Phys. Rev. Lett.* **86** (2001) 596.
[50] McLerran L, *Three lectures on the physics of small x and high gluon density* [hep-ph/9903536].
[51] Acton P D, *Z. Phys.* C **53** (1992) 539.
[52] Golec-Biernat K, these proceedings [hep-ph/0109010].
[53] Dederichs K H and Faessler M A, *Phys. Lett.* B **232** (1989) 405.
[54] H1 Collab., Adloff C *et al* , *Phys. Lett.* B **520** (2001) 183.
[55] ZEUS Collab., Breitweg J *et al* , *Eur. Phys. J.* C **6** (1999) 603, C **2** (1998) 247.